Mechanical Systems and Signal Processing 235 (2025) 112879

Contents lists available at ScienceDirect

Mechanical Systems and Signal Processing

journal homepage: www.elsevier.com/locate/ymssp

Full Length Article

Robustness in the dynamic response of turbine blades with under-platform dampers

Alfredo Fantetti [a,*], Tom Mace [a], Adrian Jones [b], Christoph Schwingshackl [a]

[a] Department of Mechanical Engineering, Imperial College London, Exhibition Rd, SW7 2BU, London, UK
[b] Rolls Royce plc, UK

ARTICLE INFO

Communicated by X. Jing

Keywords:
Under-platform dampers
Jointed structures
Nonlinear dynamics
Friction hysteresis loops
Experimental uncertainty

ABSTRACT

This article investigates the sources of uncertainty in the dynamic response of turbine blades equipped with under-platform dampers (UPDs). While UPDs play a critical role in energy dissipation and vibration control, their effectiveness is influenced by various uncertainty factors, including contact pressure distribution, manufacturing variability, wear, loading history and many others. Among these, uncertainty due to initial loading conditions and assembly procedures is particularly significant, as small variations in the damper's positioning lead to measurable differences in the system's response. Through a combination of experimental testing and numerical simulations, this study quantifies these effects and provides practical guidelines for improving the reliability of both measurements and simulations. The findings highlight the need for UPD designs that minimize assembly-induced variability, and stress the importance of accurately matching experimentally measured pressure distributions with numerical models.

1. Introduction

Turbomachinery and other aero-engine structures are constructed from thousands of assembled components, resulting in a great number of contact interfaces. During operation, vibration induces relative motion at these contact interfaces, leading to energy dissipation through friction. While this frictional damping is beneficial for reducing vibration amplitude, it can also cause wear, potentially compromising component integrity. With the help of state-of-the-art modeling techniques, frictional damping can be maximized while wear is purposely designed to only occur in less critical areas, resulting in safer and more efficient designs [1,2]. In turbomachinery, typical contact interfaces include turbine blade roots [3–5], shrouds [6–9] and also specifically designed damping devices such as under-platform dampers (UPDs) [10–14]. UPDs are small metal masses positioned beneath the platforms of adjacent turbine blades. Due to centrifugal forces during engine operation, these dampers are pressed against the blade platforms, facilitating energy dissipation through frictional interactions occurring during vibration. These frictional interactions introduce strong nonlinearities into the dynamic response of turbine blades, causing both vibration amplitudes and resonance frequencies to depend on the excitation level. To capture these effects, researchers often couple high-fidelity Finite Element (FE) models with nonlinear contact elements, such as the Jenkins, Iwan, or Bouc–Wen models [15]. These may connect individual FE nodes [1] or larger contact patches [16] to balance accuracy and computational cost. Nonlinear dynamic analyses are then performed using either time-domain integration for transient behavior or frequency-domain techniques, such as the multi-harmonic balance method, for efficient steady-state response prediction [17].

While current models can predict nominal configurations reasonably well, it is more challenging to accurately replicate the behavior of real components [18]. Challenges arise due to the sensitivity of contact conditions to factors such as manufacturing

* Corresponding author.
E-mail address: a.fantetti@imperial.ac.uk (A. Fantetti).

https://doi.org/10.1016/j.ymssp.2025.112879
Received 19 March 2025; Received in revised form 9 May 2025; Accepted 18 May 2025
Available online 31 May 2025
0888-3270/© 2025 The Authors. Published by Elsevier Ltd. This is an open access article under the CC BY license (http://creativecommons.org/licenses/by/4.0/).

tolerances, assembly procedures, load uncertainties, and wear, amongst others [19–22]. These sources of variability often result in poor repeatability of the dynamic response, leading to unpredictable frictional behaviors. Given this inherent uncertainty, experimental testing and model validation are crucial.

Several experimental studies have investigated the physics of contact interfaces under vibration [11,23–26], providing valuable insights into their dynamic behavior. One key finding is the significant influence of the contact pressure distribution on the overall system response [12,22,27–32]. For instance, it was recently demonstrated in [28] that, even in a complex industrial test case such as a real aero-engine turbine disk equipped with UPDs, nonlinear dynamic predictions can closely match experimental results when contact conditions and real pressure distributions are accurately captured. Wall et al. [29] examined the impact of surface topography variations, showing that different surface roughness profiles significantly affect jointed structure dynamics. Similarly, Pesaresi et al. [12] validated a turbine blade-UPD dynamic model by explicitly representing the contact pressure distribution using a high-resolution 3D friction element grid combined with multi-harmonic balance solvers. Since the investigated UPD exhibited slight convexity due to manufacturing processes, their study highlighted the strong dependence of results on the resulting non-uniform contact pressure distribution. By incorporating pressure distribution data from pressure-sensitive films, they achieved improved correlation between numerical predictions and experimental frequency response functions. However, even with precise modeling, experimental repeatability often remains poor [19] due to additional factors such as machining tolerances [20,21], mistuning effects [33], non-uniqueness of contact forces [34,35], shaft-disk-blade coupling vibrations [36,37], and wear [38], which are difficult to incorporate into numerical models.

Gastaldi et al. [20] experimentally demonstrated that flat-on-flat contacts introduce uncertainty in UPD performance due to deviations from ideal planarity caused by manufacturing imperfections. They suggested that tighter profile tolerances could enhance the predictability of contact behavior. Similarly, Panning et al. [39] reported that wedge UPDs with flat contact interfaces are impractical due to difficulties in achieving full contact and precise mounting. Manufacturing tolerances and inappropriate contact angles can in fact cause dampers to lift at the edges, leading to multiple possible contact configurations and cyclic impacts during vibration cycles.

The assembly procedure has also been identified as a critical factor for ensuring repeatability. Brake et al. [21] showed that assembly-induced variability often exceeds the frequency shifts caused by joint nonlinearity. Wen et al. [40] conducted a thorough experimental and numerical study on the effect of machining deviations and contact parameters on the nonlinear dynamic response of a fir-tree bladed-disk structure. They showed that the impact of rough interfaces on modal characteristics is the most significant, followed by machining deviations, while the effects of assembly deviations and blade mass deviations are relatively weak in comparison. Another source of variability is the non-uniqueness of contact forces [34,35], which leads to different static force equilibria under the same nominal conditions. To account for this variability, Ferhatoglu et al. [41] developed an optimization algorithm including the uncertainties coming from UPD misalignment during assembly and loading procedures, which are found to have a large impact on the repeatability of the response. Our present study confirms these findings by providing numerical quantification and further experimental evidence. Recently, Gola [42] proposed a novel approach for UPD geometry design based on an algorithm that ensures force and moment equilibrium for given geometries. This approach could be used to design more robust UPD geometries based on mathematical and geometrical formulations.

Other significant sources of uncertainty in bladed disks are mistuning [36], which can introduce coupled resonances and lead to large variations in response amplitudes, and wear, which alters interface geometries over time impacting the pressure distribution and dynamic behavior [38,43,44]. To account for these uncertainties, some studies have employed uncertainty quantification techniques, predicting frequency response bands [45–47] with promising results. However, they either rely on time consuming (and case-specific) Monte Carlo simulations or are applied to simpler systems that do not capture all the experimental uncertainties of larger industrial structures. Thus, their application to complex systems remains an open challenge [46].

Localized measurements of contact interactions between turbine blades and UPDs [11,24] have also provided preliminary validation of nonlinear dynamic solvers. Additionally, various small-scale experimental studies on turbine bladed disks [10–12,24, 46,48,48–55] have been conducted, along with investigations on industrial-scale systems [39,56–58]. These studies highlight the critical challenge of poor joint repeatability due to the extreme sensitivity of the dynamic response to multiple, interacting factors, such as pressure distribution, assembly-induced variability, manufacturing tolerances, loading setup, and wear. Despite advances in numerical techniques, the inability to control or accurately represent these factors in experiments remains a bottleneck in predictive modeling.

In this context, the present study proposes a novel combined experimental–numerical approach to quantify and isolate the key drivers of uncertainty, with particular attention to the role of contact pressure distributions and loading configurations in turbine blades equipped with UPDs. Experiments are conducted on an in-house test rig, addressing challenges related to repeatability and the replication of experimental results with numerical models. Based on the presented results, we propose guidelines to account for these sources of uncertainty in the models, and minimize them in the experiments. By addressing these aspects, we aim to enhance the robustness of both measurements and simulations, and contribute towards more reliable predictions of nonlinear dynamics in turbomachinery components.

2. Modeling approach used to predict the nonlinear dynamic response

Various modeling techniques have been developed over the years, with the most common approach involving finite element modeling of the contacting components coupled with specialized contact models that capture friction mechanisms. The whole system is then commonly solved with multi-harmonic balance solvers [1,59]. In this article, we follow this standard approach, using the

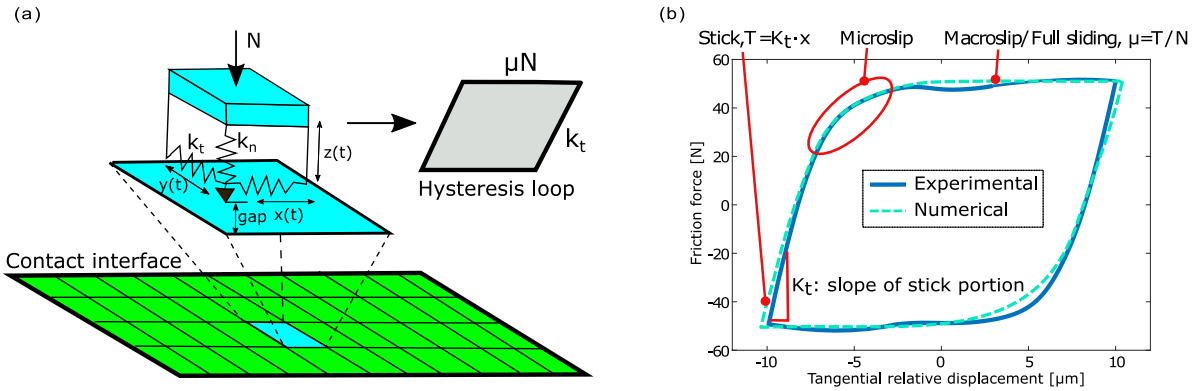

Fig. 1. (a) Example of a discretized contact interface with a 3D node-to-node Jenkins element and resulting friction hysteresis loop; (b) Comparison of one experimental hysteresis loop with a numerical hysteresis loop obtained from a contact interface discretized with several Jenkins elements [47]. The loops present microslip, which results from the gradual transition from stick to gross slip, i.e. some jenkins element fully stuck and some in gross slip.

nonlinear dynamic solver described in detail in [59]. The solver couples the multi-harmonic balance-method with an alternating time/frequency technique [60] to solve the following equations of motion:

$$M\ddot{\mathbf{x}}(t) + C\dot{\mathbf{x}}_{(t)} + K\mathbf{x}_{(t)} = \mathbf{F}_{\mathbf{ex}(t)} + \mathbf{F}_{\mathbf{nl}(t,\mathbf{x},\dot{\mathbf{x}})} \tag{1}$$

where M, C and K are respectively the mass, damping and stiffness matrices of the FE models; $\ddot{\mathbf{x}}, \dot{\mathbf{x}}, \mathbf{x}$ are the unknown acceleration, velocity and displacement of each degree of freedom respectively, which need to be computed; $\mathbf{F}_{\mathbf{ex}}$ is the vector of external forcing acting on the assembly; $\mathbf{F}_{\mathbf{nl}}(t, \mathbf{x}, \dot{\mathbf{x}})$ is the vector of the nonlinear friction forces predicted by the contact elements between each node pair representing the contact interfaces.

The problem represented by Eq. (1) is expressed in the time domain and, assuming that the excitation is periodic, it is possible to convert it in the frequency domain by applying the Multi-Harmonic Balance Method (MHBM) [59], leading to a much reduced computational cost. In the frequency domain, displacements $\mathbf{x}$(t) and nonlinear friction forces $\mathbf{F}_{nl}$ are approximated by a truncated Fourier series with n harmonics:

$$\mathbf{x}(t) = \mathbf{Q}_0 + \sum_{j=1}^{n} \mathbf{Q}_j^c \cos(j\omega t) + \mathbf{Q}_j^s \sin(j\omega t) \tag{2}$$

where $\mathbf{Q}_0$ is the 0th order harmonic coefficient, $\mathbf{Q}_j^c$, $\mathbf{Q}_j^s$ are the jth harmonic coefficients (cosine and sine components respectively) for each DOF, and ω is the excitation frequency. In the present study, the only harmonic coefficients included in the simulations are the first, second and third harmonic of the excitation frequency. The zero harmonic is not included in the simulations and, as a result, the static equilibrium is assumed to be invariant throughout each vibration cycle. Future follow-up work will however consider also the effect of the zero harmonic.

The system of algebraic Eq. (2) is then solved with a Newton–Raphson solver [1,59,61]. The challenge thereby is that both friction forces and displacements are unknowns in the equation of motion. The friction forces are estimated for each contact node pair via the contact elements through an alternating time/frequency technique, which is commonly used in combination with the MHBM [60]. The nonlinear elements chosen in this work are 3-directional Jenkins contact elements [62], which are shown in Fig. 1a. The 3D Jenkins element is composed of a slider that defines the friction limit at which gross slip occurs, equivalent to the friction coefficient, μ, multiplied by the normal load acting on the analyzed contact node pair. Additionally it features three springs representing the normal stiffness, k_n, and the two tangential contact stiffnesses, k_t, originating from the elastic deformation of the asperities in contact. The two contact nodes connected by a 3D Jenkins contact element can experience stick, gross slip or separation during a vibration cycle. Fig. 1a shows a Jenkins element and an example of a hysteresis loop. When the contact interface is discretized with several Jenkins elements, some may stick and some may slip leading to microslip as shown in Fig. 1b.

3. Test case: the under-platform damper rig

The test rig used for this study represents a simplified blade-damper geometry. It consists of two beam-like turbine blades equipped with an under-platform damper (UPD) [12]. The two blades are manufactured with a common base (Fig. 2a), which is clamped securely to a machine bed with a hydraulic ram. This setup reduces the number of undesirable joints, to isolate and study primarily the friction nonlinearity in the UPD/blade contact interfaces, whilst reducing the effects of the boundary conditions.

The UPD is loaded beneath the blade platforms via two steel cables which pass through two through-holes in the damper and transmit a load to the bottom surface of the damper with a crimped brass ferrule (Fig. 2b–c), approximating the centrifugal forces encountered during turbine operation. The load is applied using a chainblock and measured with a weighing scale (Fig. 3). This loading system is an improvement over that of the original rig [12], and enables the application of pulling loads larger than 1000 N,

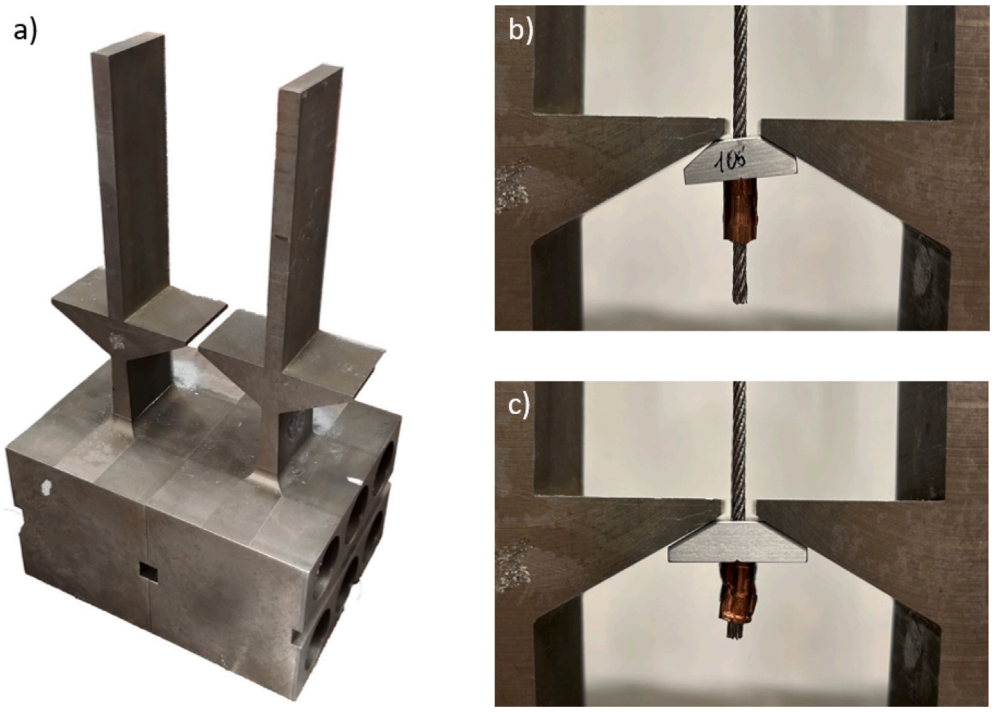

Fig. 2. (a) Turbine blade assembly of the UPD test rig; (b–c) Two UPD geometries used in this study.

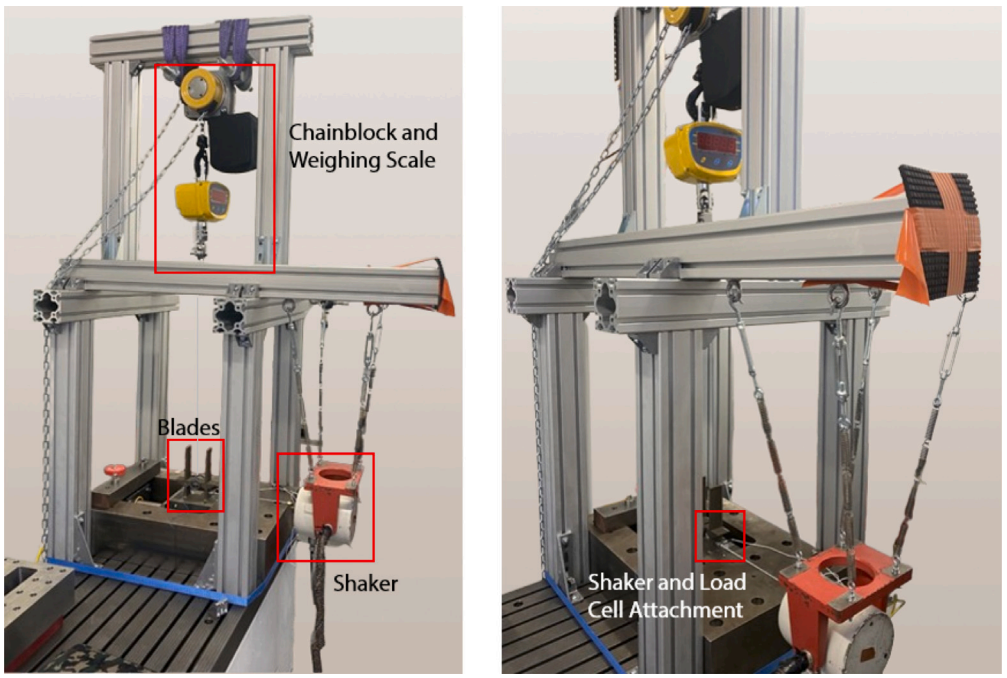

Fig. 3. UPD rig with the shaker hanging on springs and attached to the base of one blade via a load cell.

also facilitated by the stronger metallic frame supporting the chainblock. A series of hammer tests was performed to verify that the rotational stiffening induced by the pulling wires is negligible even at larger pulling loads. Those tests, not shown here, suggested that such stiffening has negligible effects on the UPD motion for the investigated vibration modes.

Excitation and instrumentation. The structure is excited with a DataPhysics Signalforce 100 W shaker system suspended on springs to decouple the shaker itself from the machine bed where the blades are mounted. The shaker is attached to the base of one blade with a stinger (see Fig. 3) and the excitation force is measured using a PCB 208C04 load cell, mounted between the shaker's stinger and the blade attachment location.

The blade velocity is measured with a single point Polytec VibroGo Laser Doppler Vibrometer (LDV) pointing at the blade airfoil. The frequency response function of the blade is subsequently recorded by measuring velocity and excitation force with a stepped-sine testing approach, and with a closed-loop amplitude input control, which enables the analysis of the system's nonlinear damping behavior at different excitation magnitudes. All data was captured with a DataPhysics Abacus digital acquisition system.

UPD geometry used in this study. The UPDs used in this study have a wedge-like shape that leads to an edge contact with one blade platform (left contact in Fig. 2b) and a face in full contact with the other blade (right contact in Fig. 2b). This wedge-like shape was designed as part of a larger industry-driven project, focused on the improvement of UPD designs for achieving better dynamic performances [63]. The two designs employed in this article are shown in Fig. 2b–c. These UPDs geometries can only experience the following two configurations: (1) face contact on left side and edge contact on right side or (2) edge contact on left side and face contact on right side. In the current test rig, the UPD would always self-align in just one of the two configurations, guided by the attachment with the crimped brass ferrule that transmits the pulling load from the wires (see Fig. 10). While the configuration is univocal in this test rig, in real applications – where the UPD is not guided by the ferrules, but instead driven by the centrifugal load – there is a risk that the UPD may settle into the opposite configuration once the engine starts. Hence, designs that impede such switching between configurations, such as those proposed in [39,42], may offer greater robustness for this purpose, unless future studies demonstrate that such switching provides additional damping, which would be beneficial for vibration reduction.

3.1. Finite element model

The finite element (FE) model of the rig is shown in Fig. 4a and has been described in detail and validated in [12]. Blades and UPD were generated with approximately 60,000 quadratic hexahedral elements, and the material properties of the stainless steel were used (E = 197 GPa, ρ = 7800 kg/m^3). Particular care was taken during the meshing process to guarantee matching nodes between the blade platforms and UPD faces. A total of up to 146 interface nodes were created with every FE node covering roughly 0.3 mm^2, enabling a good discretization of the contact area while keeping an acceptable computational time, as suggested in previous studies [28,64]. The dynamic contact behavior of each interface node was modeled with the 3D Jenkins elements described in Section 2.

To simulate the shaker excitation, a single harmonic excitation is applied to the closest node corresponding to the experimental attachment of the shaker to the blade base. Similarly, the velocity response of the blade is evaluated near its tip, where the LDV is pointing at during the experiment, as shown in Fig. 4a. The pulling load coming from the wires is simulated through two point loads applied at the UPD base through a quasi-static simulation in Abaqus. Fig. 4b shows an example of the resulting contact pressure on both edge and full contact sides of the UPD for a pulling load of 1000 N, which is large enough to ensure a good conformity at

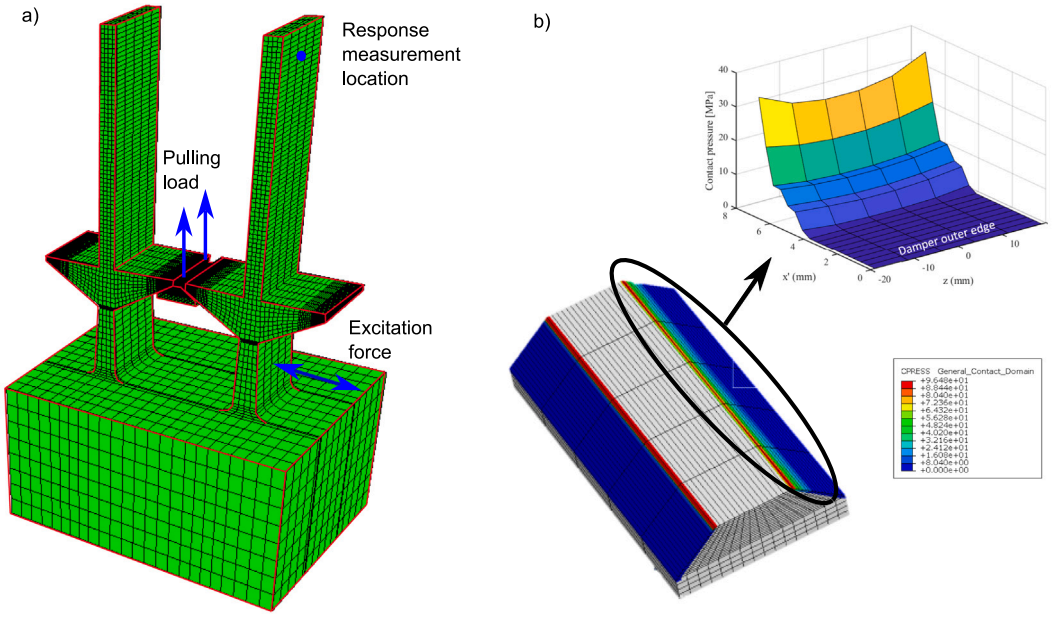

Fig. 4. (a) Finite Element Model of the UPD Rig and (b) example of the contact pressure distribution on the UPD.

the contact interface since an initial convergence study showed strong joint variability at lower damper loads [12]. For the full-face contact, the contact pressure is maximum on the inner edge of the UPD and almost zero on the outer edge. This non-uniform pressure distribution will be accounted for in the nonlinear dynamics simulations. On the edge contact side, the pressure is almost constant along the edge, around 10 MPa. Depending on the actual contact distribution, the dynamic response is stiffer or softer, as will be demonstrated in the following sections.

The pressure distribution obtained from Abaqus is then used to extrapolate the normal load acting on every UPD/blade interface node. The normal load is needed as input for the Jenkins element connecting every node pair in the nonlinear dynamic solver. The other contact parameters used as input for the Jenkins are the friction coefficient, μ, equal to 0.8 for all nodes based on previous hysteresis measurements from a in-house fretting rig [65,66], which is smaller than the friction coefficient of 0.6 usually used in the literature. The pressure-dependent tangential contact stiffness, k_t [N/mm^3], is also obtained from experimental measurements with the following law, $k = 315\,000^*\sqrt{p}$, where p is the contact pressure on the node in MPa [67]. The normal contact stiffness is considered 1.25 larger than k_t according to contact mechanics [68]. The effect of these contact parameters on the nonlinear dynamic response has been investigated in previous studies and it is not the object of the present investigation [28].

4. Numerical dynamic response of the under-platform damper test rig

The first flexural mode (1F) is investigated in this study since it is the target mode for vibration dampening through the use of the UPD. Due to the double-blade configuration of the rig with a single damper in between, two 1F modes are excited, the in-phase (IP) and out-of-phase (OOP), with the two blades moving respectively in phase and out of phase.

To show the impact of the UPD on these two modes, simulations were performed at several excitation amplitudes with the MHBM dynamic solver described in Section 2. The simulated Frequency Response Functions (FRFs) are reported in Fig. 5, which shows that the two modes have different resonance frequencies, with the IP mode being softer, as commonly known in the literature. The response damps significantly for the OOP mode as the excitation amplitude increases, highlighting the effectiveness of the UPD in reducing the vibration amplitude. Also the IP damps, but to a lower extent. In the OOP mode, the UPD is more effective since the OOP mode is characterized by a sliding motion of the UPD with the blade platforms, while during IP motion the damper mainly rolls with the platforms, although at the same time it slides on the platform surfaces by an amount that depends on the contact angles. Thus, the effectiveness of damping on IP or OOP modes depends on the UPD shape. The tendency of the damper to roll also explains why this mode is softer since, at higher amplitudes, the contact area at the UPD-platform interface may reduce, leading to a continuously changing and softer system [12]. At larger excitation amplitude, the IP mode shows a softening behavior induced by larger rolling that leads to further detachment and impacts between the UPD and the blade platforms.

Previous studies have shown that the real contact pressure distribution is often non-uniform and must be accurately represented in simulations [28]. For example, Abaqus simulations in Fig. 4b predict highly non-uniform pressures. In this study, the UPD geometry features a face contact on one side and an edge contact on the other (see Fig. 2b). To assess the impact of different pressure distributions, we simulated several contact cases on the face side ranging from partial to fully distributed contact.

In the fully distributed contact case (a common assumption in the literature, though not always realistic), all 17 lines of finite element nodes across the face were included in the simulation, as illustrated in the "Nominal full contact" schematic in Fig. 6. The opposite side of the UPD, by design, only allows for edge contact. The specific contact edge (inner or outer) depends on the UPD shape. This article focuses on two geometries with inner edge contact, but similar trends were observed for UPD designs with outer edge contacts.

For partial contact simulations, we progressively reduced the number of active contact lines (e.g., 1, 3, or 11 lines), following the method from [28] and shown in Fig. 6. We ran simulations for both inner and outer edge contacts on the face side, while keeping the edge side fixed with inner edge contact.

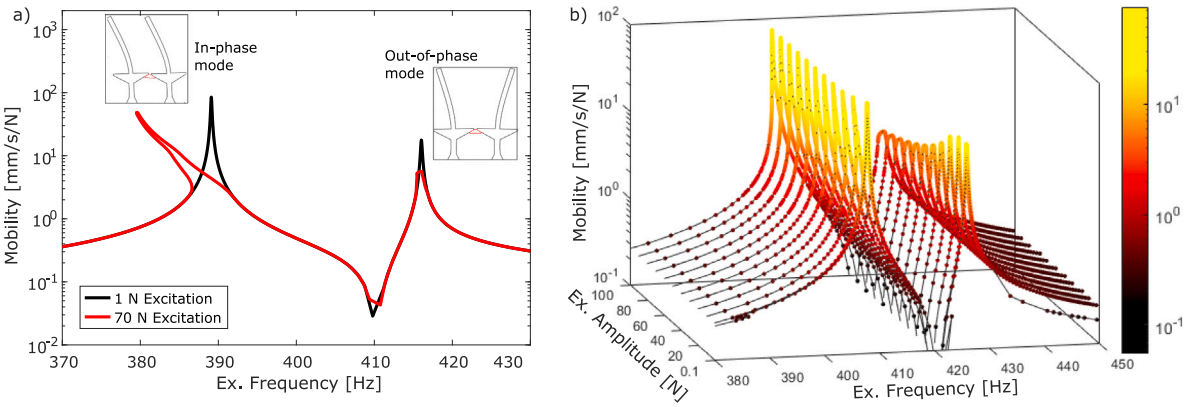

Fig. 5. Numerical FRFs showing IP and OOP modes under (a) two low and high excitation amplitudes and (b) wider range of excitation amplitudes.

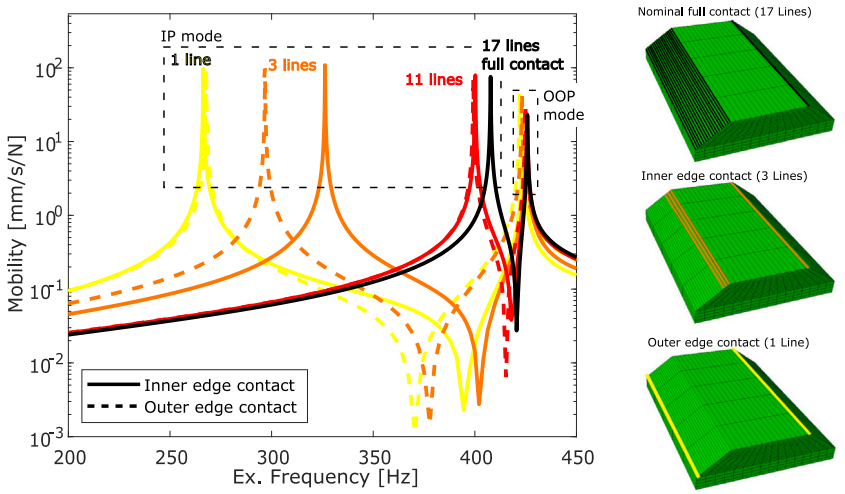

Fig. 6. Numerical FRFs obtained for the UPD type shown in Fig. 2c under different contact pressure distributions with 1 N harmonic excitation and 1000 N pulling load.

FRF simulations are shown in Fig. 6 for these cases. The contact distribution affects significantly the IP mode: the wider the contact (from 1 to 17 lines of contact included), the stiffer the response, with a remarkable 40% increase in the resonance frequency. The OOP mode is more robust against changes in the extension of the contact, with increases in the resonance frequency below 3%. The higher robustness of the OOP mode can be due to the larger amount of sliding motion typical of that mode, which probably allows the contact pressure to settle to a more consistent value during vibration cycles. Instead, the IP mode is characterized by a rolling motion, which is more dependent on the initial conditions and, particularly, is stiffened by a wider contact distribution that prevents the UPD rotation typical of the IP mode. This large effect of the pressure distribution on the IP mode resonance frequency should be accounted for when designing new UPD geometries or testing them.

For the face contact side, Fig. 6 shows inner edge and outer edge contacts. For both cases, the behavior is similar as long as the contact lines included in the simulations are the same, except for the 3 lines contact case. This similarity indicates that, for the IP mode, the extension of the contact area has a larger effect than the actual contact location, inner or outer edge. In fact, the UPD has a lot of compliance to rotate regardless of the contact being on the outer or inner edge. Instead with the nominal case, the full interface is prevented from rotation, thus stiffening the mode. The OOP mode seems to be instead insensitive to both extension and distribution of the contact area, as it does not show rotation, but mainly sliding due to the kinematics of the blades moving out of phase, at least for the investigated UPD geometry.

To provide more insights into the kinematics of the two modes and validate the previous statements, we also analyzed the contact conditions at the resonance frequency for every contact case and for both modes. Fig. 7 shows, as an example, the contact conditions of IP and OOP modes for the full contact case (17 contact lines on full contact side) under a large 70 N harmonic excitation. Due to the very large excitation force, all the contact nodes at the IP mode resonance frequency show a separation state (we define a separation state if, within the vibration cycle, the contact nodes separate at least in one time instant). The separation is expected as the IP mode is characterized by a rolling motion that implies node separation within a vibration cycle. The separation of the individual contact node pairs occurs at different time instants based on the rotation kinematics. Note that with a low 1 N excitation, not shown in the figure, all the contact nodes are in a fully stuck condition. The OOP mode shows fewer nodes in separation, while more nodes are either in stick condition (black) or in slip condition (blue). Particularly, all the nodes at the edge contact are slipping, meaning that while the full contact face is mainly stuck, while the edge side slips against the blade in contact with it. This amount of sliding leads to the damping that is beneficial to reduce the vibration of the blades. Tables A.1 and A.2 in the Appendix show the contact conditions of IP and OOP modes for all the contact line cases under the two different excitation amplitudes. To further understand the effect and repeatability of the contact pressure and validate the preliminary insights from these simulations, the experiments detailed in the following section have been performed.

5. Uncertainty of experimental data

Two UPD geometries are investigated in this study, shown in Fig. 2b-c. The first UPD was loaded to a 1000N pulling load with the chainblock. Then, a shaker sweep was performed to measure the FRFs. The blade velocity was measured with a single laser doppler vibrometer on the top of one of the two blades, in the location shown in Fig. 4a. Fig. 8a shows three FRFs measured one after the other with down frequency sweeps, from high to low frequencies. They are repeatable, indicating that dynamic response, for a given assembly, is repeatable. As expected, the IP and OOP modes are visible in the frequency range of interest, with the IP mode being softer. Note that these FRFs, and the rest of the FRFs shown in this section, are in a steady state condition after an initial running in, which is commonly observed when two components come in contact for the first time. Particularly, to ensure the

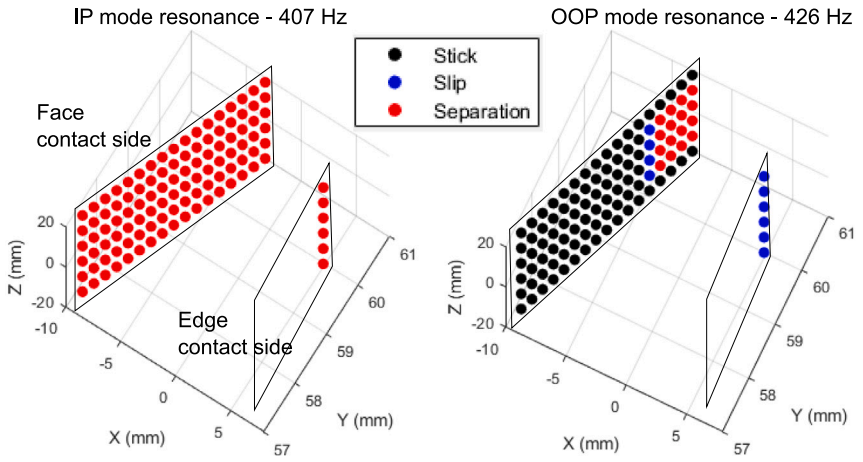

Fig. 7. Contact conditions at IP and OOP mode resonances respectively, with excitation level of 70 N and 17 lines of contact included in the simulation for the face contact side.

contact settled to a stable state, the blades were excited continuously for 5 min at the OOP resonance ensuring some UPD/blade platform relative motion. During such running in, resonance frequencies changed by up to 10 Hz for the IP mode and up to 1 Hz for the OOP mode before settling in. Resonance amplitudes changed up to 30% for the IP mode and 10% for the OOP mode, with most of the variation occurring within the first minute of excitation. Fig. 8a shows that the response is stable after such running in.

After these first measurements, the UPD was unloaded by removing the pulling load and then reloaded by reapplying the 1000 N pulling load. FRFs were measured for different assemblies after the initial running in, and are shown in Fig. 8b. Different assemblies of the same UPD lead to larger scatter in the measured FRFs, especially for the IP mode (13 Hz range from 383 Hz to 396 Hz), while the OOP mode is more repeatable (resonance frequencies within a 2 Hz range). Several factors contribute to this scatter, which have been investigated and discussed in the following sections.

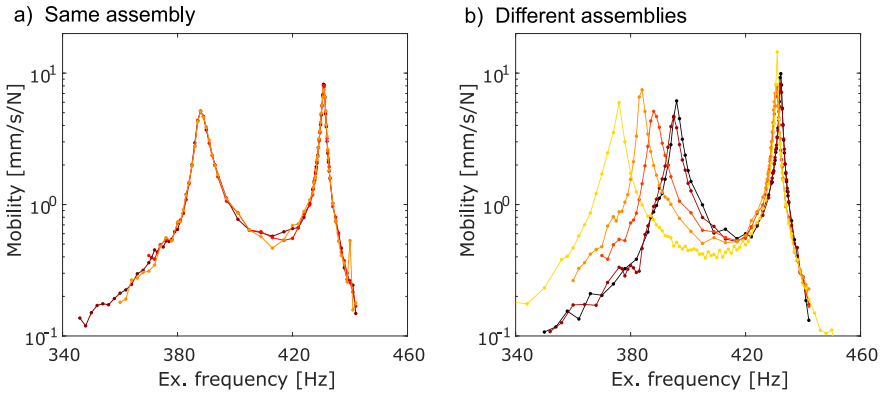

Fig. 8. Experimental FRFs: (a) three consecutive shaker sweeps for the same UPD assembly measured with 1000 N pulling load and 0.1 N harmonic excitation; (b) shaker sweeps for different UPD assemblies (i.e. UPD loading and unloading between different sweeps) measured under 1000 N pulling load and 0.1 N harmonic excitation. The change in the resonance frequency did not follow the test order, e.g. in one test the resonance frequency was large, in the next test was smaller and in the next larger again.

5.1. Effect of pulling wire loading on the repeatability of measured FRFs

A possible reason for the high variability in the measured FRFs could be the pulling load, 1000 N, which leads to a relatively low contact pressure of about 3 MPa (since the nominal area of the UPD was about 300 mm^2, assuming full contact on one side and edge contact on the other). Note that UPDs in aero-engines experience pressures up to 30 MPa, i.e. one order of magnitude more. Because of this low pressure, contact interfaces might not settle in the same position for the different experiments. To verify this hypothesis, experiments with a 4000 N pulling load were performed for different assemblies. Fig. 9a shows FRFs for different assemblies with 4000 N pulling load, but it is clear that the repeatability has not improved. Indeed, resonant frequencies of the IP mode still lie within a range of 12 Hz, which is the same scatter as in Fig. 8b. Hence, the low contact pressure does not seem to be the cause of this low repeatability.

During those experiments, another possible influencing factor was identified. By visually inspecting the assemblies, it was observed that the loading wire was slightly touching the UPD hole in the case of tests with the highest IP resonance frequency (see e.g. test 1 in Fig. 9b). Probably, the wire touching the UPD hole constrains the UPD rotation, which is typical of the IP mode, as visualized in the scheme of Fig. 10b. To further prove this hypothesis, more tests were performed by carefully placing the wire in the center of the hole, ensuring that there was not contact with the UPD, see tests 2–6 in Fig. 9b. Only for test 1, the wire was purposely put in contact with the UPD. FRFs are shown in Fig. 9a, in which the test 1 has the stiffest IP resonance frequency. Excluding that test, the other FRFs lie within a 5 Hz range. Note that the resonant frequency of the OOP mode is instead mostly unchanged, even in the case of wire contact. This probably occurs because, during the OOP motion, the UPD moves rigidly with the wire, up and down as shown in Fig. 10c, and thus it is not constrained by the contact with the wire.

This effect of the wire loading has not been reported before, but it should be treated with particular care since the use of wire loading is a very common loading system used in UPD rigs [10–12,24,49–53], and this effect cannot be neglected. Possible solutions to minimize this problem are the visual inspection of the assembly before running the experiment, the use of different loading systems (e.g. through a knife edge, or with non-contact techniques) or using thinner wires or larger through-holes if they can sustain the expected loads.

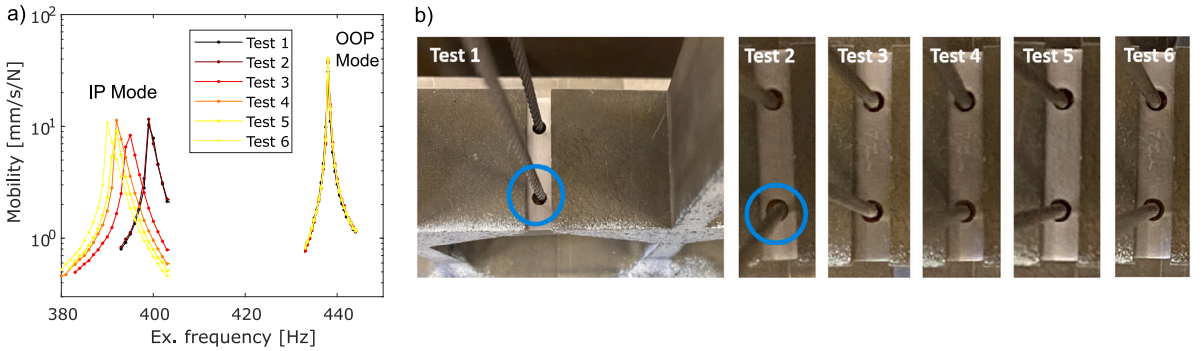

Fig. 9. (a) Shaker sweeps for different UPD assemblies (i.e. UPD loading and unloading between different sweeps) measured under 4000 N pulling load and 4 N harmonic excitation; (b–c) Top view of the UPD/blade assembly to show the wire going through the UPD.

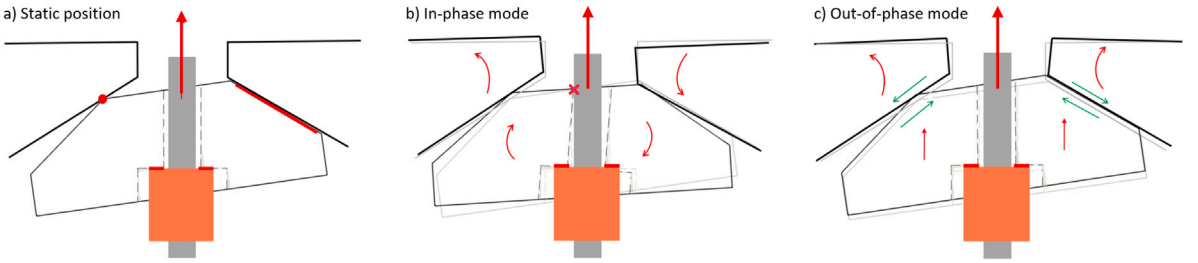

Fig. 10. Simplified scheme of the UPD wire loading: (a) static position with pulling load; (b) in-phase mode and UPD rotation – the wire might touch the UPD through hole; (c) out-of-phase mode and UPD vertical movement – the wire moves rigidly with the UPD and there is sliding between UPD and blades.

5.2. *Effect of the contact extension due to mounting and assembly*

After identifying the wire problem, new measurements were performed on the second UPD geometry of this study, shown in Fig. 2c. This geometry exhibits a resonance frequency with very poor repeatability, as predicted by an optimization algorithm developed to find the most robust UPD designs against manufacturing uncertainties [63]. The reasons for the poor repeatability are due to the UPD angle, which is very similar to the angle between the blade platforms and, thus, is more sensitive to small misalignments. To test the repeatability of this UPD geometry, FRFs were measured for different assemblies (i.e. after unloading and re-loading the UPD at a 1000 N pulling load), ensuring that the wire was not touching the side of the holes in the UPD. For this UPD, a much larger scatter was observed in the IP resonance frequency, with values ranging from 270 Hz up to 370 Hz, i.e. up to a 40% increase. The OOP mode was instead more stable with resonance frequencies within 5 Hz. Since the large frequency shift of the IP mode could not be attributed to the wire loading, which was carefully checked, it was hypothesized that the contact pressure distribution was drastically different in each assembly. The simulations of Fig. 6 showed in fact that, for that particular UPD geometry, different pressure distributions lead to changes in the IP resonance up to 150 Hz.

To validate this hypothesis on the pressure distribution, the actual contact pressure was experimentally measured with pressure film for different assemblies of the same UPD. The pressure films were placed between the UPD and the blades as shown in Fig. 11a, on both the full face side and edge contact sides. After applying the pulling load, the UPD was unloaded and the pressure films showed color gradients indicating the amount of pressure along the interface. Fig. 11b shows the pressure measurements for two different assemblies of the investigated UPD. For both assemblies, the edge contact shows a uniform pressure along the edge.

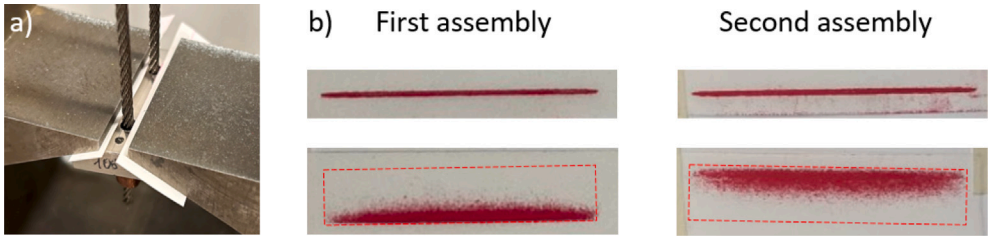

Fig. 11. (a) UPD and blade platforms with a pressure film; (b) Pressure film measurements of two different assemblies of the same UPD (that shown in Fig. 2c). For both assemblies, one pressure film shows the edge contact pressure and the other shows the contact pressure on the full face side (with the nominal area red-dashed). The pressure range of each pressure film is 0.62–9.65 MPa.

However, the face contact shows two completely different pressure distributions. For the first assembly, there is contact towards the outer edge of the UPD, while for the second assembly, there is contact on the inner edge of the UPD.

This difference probably occurs due to the inherent uncertainty in the mounting procedure for this particular UPD geometry, which in fact was defined as non-robust by the optimization algorithm [63]. The reason is attributable to the angle of the UPD, which is similar to the angle between the blade platforms and thus is more sensitive to small misalignments, as for example observed in [41]. This mounting uncertainty could have an impact also in real applications since, in operating turbines, UPDs sit freely below the blade platforms, and they contact the blades at different locations when pushed by the centrifugal loading under engine operation. As such, the pressure distribution might not be repeatable, depending on the first point of contact between UPD and blade platform, given the UPD's freedom of movement before the contact.

It should be noted that, in this study, the contact interfaces of the UPD and blade platforms were also scanned with a microscope to verify whether or not any variation from the nominal design could affect the pressure measurements. The measured flatness of each contact interface was lower than 15 μm, which is considered acceptable since 20 μm is the smallest flatness value defined in the standard ISO 2768 general tolerance specification [69].

To relate the measured pressure distributions to the corresponding FRFs, hammer tests were performed while a pressure film was in place between the UPD/blade interface. Note that this test provides qualitative results only, as the pressure films add compliance at the interfaces and would be expected to change the dynamic response. Several assemblies at 1000 N pulling loads were tested by unloading the UPD, placing a new pressure film and re-loading to 1000 N on every iteration. With the pressure film in place, hammer tests were performed rather than shaker sweeps, since they are significantly faster tests to undertake. At the end of each test, the UPD was unloaded and the colors on the pressure films were examined.

Fig. 12 shows the three most representative dynamic responses and their corresponding contact pressure distributions. As already observed with the preliminary shaker sweeps, the hammer tests performed with pressure films in place also lead to 100 Hz frequency shifts in the IP resonance, while the OOP resonance frequency is much more repeatable with changes within 5 Hz. The stiffer IP resonances correspond to tests in which the pressure films had more distributed contact pressure distributions, while tests with edge-like pressure distributions had the softest responses. When similar pressure distributions were achieved in different assemblies with different pressure films, the differences in the resonance frequencies were below 1 Hz for the IP mode and 0.1 Hz for the OOP mode, not shown in the Figure.

It is clear from this example that the extension of the contact distribution strongly affects the resonance of the IP mode: the wider the contact, the stiffer the response. The OOP mode is more robust against changes in the extension of the contact. This is in strong agreement with the preliminary simulations of Section 4, which are compared to the experiments in the next section.

6. Comparison of experiments and simulations

Fig. 13 shows a comparison of IP and OOP resonant frequencies obtained from the numerical simulations shown in Section 4, for different pressure distributions, and the experimental FRFs from the previous section. Note that this comparison is only qualitative since the pressure films add compliance at the interfaces that has not been modeled in the simulations. In addition, the simulations were performed assuming a sine sweep with 1 N excitation amplitude, while the measurements were performed with hammer tests with impacts around 100 N. While the shaker excites the blade at its base, the hammer impact was performed above the platform, on the blade airfoil, due to a lack of available space. The different excitation point, in combination with the not-modeled-compliance from the pressure films, resulted in experimental and numerical amplitude responses differing by one order of magnitude. Thus, the amplitude comparison is not discussed in this section.

Instead, the comparison of experimental and numerical resonance frequencies in Fig. 13, whilst qualitative, shows excellent correlation in support of the authors' hypotheses. Trends are similar for both experiments and simulations, with resonance frequencies increasing as the contact distribution extends, especially for the IP mode (increases up to 40% in the resonance frequency). The OOP mode is more robust against changes in the extension of the contact, with increases in the resonant frequency below 3%. For both IP and OOP modes, the experimental resonances fall within 3% of the predicted values, which is deemed acceptable given the presence of pressure films during the measurements. We also modeled even more realistic contacts by selecting

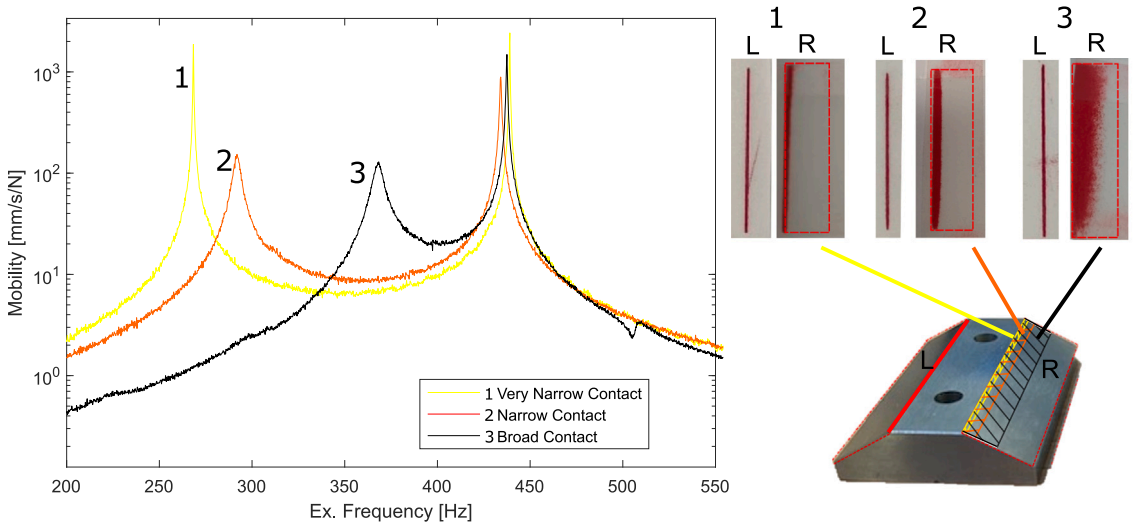

Fig. 12. FRFs obtained from hammer tests for different UPD assemblies (i.e. UPD loading and unloading between different tests) measured under 1000 N pulling load, and with pressure films placed between UPD and blade platforms during the test.

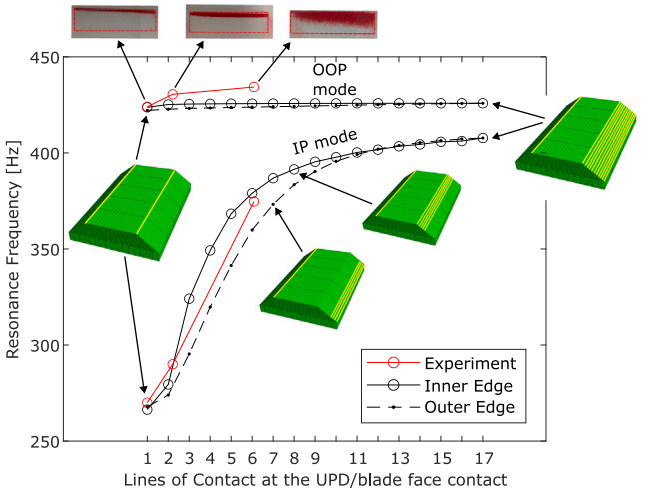

Fig. 13. Comparison of the resonance frequencies of IP and OOP modes from the numerical simulations of Fig. 6 and experimental FRFs of Fig. 12, both performed with pulling loads of 1000 N.

the exact nodes in the numerical model that matched the contact zone geometry measured using pressure films. However, since the results did not differ significantly from the 'full-line' simulations, only the latter are shown in the figure for clarity.

Additionally, the Figure also shows numerical FRFs for cases not observed during the experiments, i.e. more extended areas of contact up to the full uniform contact with all the 17 lines of contact included in the simulation, as well as the outer edge contact pressure distribution, which was not achieved within those tests. As discussed before, it seems that the location of the contact (outer or inner) does not itself lead to major different numerical results for either mode, provided that the contact extension is the same. This indicates that, for the investigated UPD geometry, the extension of the area of contact has a larger effect than the contact spatial distribution, particularly for the IP mode. Instead, the OOP mode is insensitive to both extension and distribution of the contact area, as it does not show rotation, but mainly sliding due to the kinematics of the blades moving out of phase (see Fig. 10c).

6.1. Guidelines from experiments and simulations

The main highlight of this experimental campaign for the investigated UPD geometry is that, although great care is ensured during the assembly, the UPD/blade platform contact strongly varies depending on the assembly. It has not been possible to decrease this uncertainty, nor to reliably place the damper in the same location every time, which has resulted in the observed variability in the dynamic response. It is expected that such assembly uncertainty could be even larger for real in-service applications, where UPDs are free to move before being engaged in contact with their respective blade platform once the engine speed is high enough to provide sufficient centrifugal loading. Different initial positions lead to different pressure distributions, which then result in significantly different dynamic responses. This indicates that engineers should prioritize UPD designs that minimize such uncertainty, as for example discussed in [22], where interfaces with steps are proposed which lead to higher repeatability and predictability. Based on the experiments and simulations performed in this article, the following guidelines are suggested:

- It is recommended to perform a pressure distribution sensitivity analysis in current modeling approaches for nonlinear dynamic analysis of jointed structures, instead of assuming a contact is uniformly distributed. Ideally, a range of representative contact pressure distributions should be simulated to evaluate the range of responses in addition to uniformly distributed pressure distributions, including extreme cases such as single line contacts, enforcing the contact at those locations only. In the presented simulations, the inclusion of realistic contact pressure distributions into the model led to an acceptable match in the resonance frequencies against the measured data.
- Based on the previous guideline, it is recommended to check the real pressure distributions experimentally, e.g. with pressure films or by looking at the worn interfaces after operation/testing to actually understand where the contact occurred, as done in [28] with the visual observation of worn UPDs of a real aero-engine bladed disk subjected to several running cycles.
- The extension of the contact has a larger effect than the spatial distribution of the contact spots for a given extension. For example, in the investigated UPDs, a 20% increase in the contact area led to a 6% increase in the resonance frequency, while a drastic change of the spatial distribution (e.g. from inner edge to outer edge contact) led to a minor change in the resonance frequency lower than 2%. However, this is specific for the considered UPD geometry, and different geometries could lead to different conclusions. This aspect should be investigated numerically before manufacturing new UPD geometries, by performing contact sensitivity analyses as suggested above.
- Depending on the mode kinematics, the pressure distribution might strongly affect the resonance frequency (in the IP mode), or might not (in the OOP mode). The driving factor is the kinematic motion typical of the investigated mode, e.g. if it involves mainly rotation as in the case of the IP mode, or if it involves mainly lateral sliding as in the case of the OOP mode. Modes involving rotation appear more sensitive to changes in the pressure distribution, for the UPD geometries considered in this study. This indicates that there may be benefits to alternative UPD design styles, which present geometries robust for different kinematic motions, as well as contact interfaces that are robust to different effects of geometric tolerance, wear, mode shape etc. These aspects should be the basis for future research directions.
- Finally, the UPD wire loading system should be treated with particular care since its effect cannot be neglected and is a very common loading system used in existing UPD rigs [10–12,24,49–53]. Possible solutions to minimize this problem are the visual inspection of the assembly before running the experiment, the use of thinner wires or larger through-holes if they can sustain the expected loads, or eventually the use of different loading systems (e.g. a knife edge or loading with non-contact techniques such as pressured air [55]).

Please note that these guidelines are derived from an analysis of two UPD geometries with a focus on the blades' first bending mode shape only. Specifically, the experiments presented the following simplifications with respect to a real bladed turbine disk: pulling load instead of centrifugal force, two dummy blades instead of a full bladed disk, and shaker/hammer point excitation instead of aerodynamic excitation. Yet, some of the guidelines, especially those concerning the pressure distribution, are considered general and applicable to more realistic structures as well.

7. Conclusions

This article has shown experimental measurements and numerical simulations of the dynamic response of simplified turbine blades equipped with under-platform dampers (UPD). The experiments were performed to identify key sources of uncertainty affecting the measured response. Despite careful assembly procedures, variability remained due to unavoidable differences in damper positioning and mounting conditions. In particular, we demonstrated that pressure distribution, loading configuration, and assembly repeatability significantly influence the system's dynamic behavior. Below, we summarize the main findings for the two flexural modes investigated: the In-Phase (IP) and Out-of-Phase (OOP) modes.

- The mode kinematics strongly affect the dynamic behavior: the IP mode is much less robust than the OOP mode, which instead is very repeatable against all the factors investigated. This can be due to the larger amount of sliding motion in the OOP mode, which probably allows the contact pressure to settle to a more consistent value during vibration cycles. Instead, the IP mode is mainly characterized by a UPD rotation, which probably is more dependent on the initial conditions and, hence, should be the focus of future optimization studies on robustness. Thus, for the considered UPD geometries, the pressure distribution strongly affects the resonance frequency of the IP mode, and less that of the OOP mode.

- The wire loading system, which is commonly used in UPD rigs to apply the pulling load, strongly affects the measurements if the wire touches the UPD on its sides. This aspect is often overlooked in existing studies, likely because it is not present in real applications, where instead the load comes from the UPD centrifugal load. The experiments presented here indicate that this is an important aspect to consider for reliable and accurate measurements, as it induces changes up to 10 Hz in the resonant frequency of the IP mode and 0.5 Hz for the OOP mode when the wires touch the UPD. The stiffening in the IP mode occurs since the wire constrains the UPD rotation, typical of the IP mode. To avoid this issue, possible solutions are visual inspection to make sure the wire does not touch, or using a different loading system if possible.
- Widely extended pressure distributions lead to stiffening up to 100 Hz (40% increase) for the IP mode resonant frequency. For the OOP mode, changes were within 2 Hz. These changes are probably driven by the UPD mode kinematics and by the relative phase and motion of the UPD and the blade, which are both impacted by wider or narrower pressure distributions. For example, wider pressure distributions constrain the IP typical rotation to a large extent, thus constraining (and stiffening) the UPD motion relative to the blade. In the present experiments, the different pressure distributions arose during the assembly procedure of the UPD, which is difficult to standardize since the UPD is free to move in any direction before any load is applied. As a result of these findings, it is important to not assume the contact is uniformly distributed. If possible, it is recommended to check the contact pressure experimentally and assess its effect numerically. In this article, we achieved this by measuring the dynamic response while pressure film were in place between the contact interfaces.
- For the investigated UPD geometries, the extension of the contact has a greater impact than the spatial distribution for a given extension. For example, a 20% increase in the contact area led to a 6% increase in the IP mode resonance frequency, while a drastic change of the spatial distribution (i.e. from inner edge to outer edge contact) led to a minor change in the IP mode resonance frequency lower than 2%.
- Different assemblies: the mounting procedure might lead to different pressure distributions, which have a strong impact as defined above. When the achieved pressure distribution was similar for different assemblies and the wire was not touching, the differences in the resonance frequencies were below 1 Hz for the IP mode and 0.1 Hz for the OOP mode. When the wire was touching the UPD, the IP resonance frequency shifted up to 15 Hz while, when the pressure distribution was different, the IP resonance shifted up by 100 Hz (i.e. 40% increase in the resonance value).

These findings highlight the importance of the contact pressure distribution. More studies should be performed in future to understand which factors affect the pressure distribution (e.g. load history, interface topography etc.) by experimentally measuring it either before, during or after the dynamic testing of the components. This will lead to improved predictive models for the nonlinear dynamics of jointed structures.

CRediT authorship contribution statement

Alfredo Fantetti: Writing – review & editing, Writing – original draft, Project administration, Methodology, Investigation, Data curation, Conceptualization. **Tom Mace:** Writing – review & editing, Writing – original draft, Methodology, Investigation, Data curation, Conceptualization. **Adrian Jones:** Writing – review & editing, Supervision, Resources, Funding acquisition. **Christoph Schwingshackl:** Writing – review & editing, Supervision, Resources, Funding acquisition.

Declaration of competing interest

The authors declare that they have no known competing financial interests or personal relationships that could have appeared to influence the work reported in this paper.

Acknowledgments

This study was funded by Rolls-Royce plc. The authors are grateful to Rolls-Royce plc. for giving permission to publish this work.

Appendix. Contact conditions of IP and OOP modes under different contact cases and excitation amplitudes

See Tables A.1 and A.2.

Data availability

Data will be made available on request.

Table A.1
Summary of resonance frequencies and contact conditions of the IP mode, for the different contact pressure distributions with 1000 N pulling load and 1 N and 70 N harmonic excitation amplitudes.

IP mode	1 N excitation		70 N excitation	
	Resonance freq. [Hz]	Contact state [%stick/%slip/%sep]	Resonance freq. [Hz]	Contact state [%stick/%slip/%sep]
1 inner edge	266.4	100/0/0	266.4	100/0/0
3 inner edge	324.1	66.7/0/33.3	315.9	0/0/100
11 inner edge	400.2	66.7/0/33.3	397.3	0/0/100
1 outer edge	267.8	100/0/0	267.8	100/0/0
3 outer edge	295.4	66.7/0/33.3	290.7	0/0/100
11 outer edge	399.2	83.3/0/16.7	395	0/0/100
17 full contact	407.8	100/0/0	405.9	0/0/100

Table A.2
Summary of resonance frequencies and contact conditions of the OOP mode, for the different contact pressure distributions with 1000 N pulling load and 1 N and 70 N harmonic excitation amplitudes.

OOP mode	1 N excitation		70 N excitation	
	Resonance freq. [Hz]	Contact state [%stick/%slip/%sep]	Resonance freq. [Hz]	Contact state [%stick/%slip/%sep]
1 inner edge	423.7	100/0/0	423.6	50/50/0
3 inner edge	425.4	100/0/0	425.3	75/25/0
11 inner edge	425.9	100/0/0	425.8	80.6/8.33/11.1
1 outer edge	422.1	100/0/0	422.0	50/50/0
3 outer edge	423.2	100/0/0	423.1	75/25/0
11 outer edge	425.0	100/0/0	424.9	75/8.33/16.7
17 full contact	426.0	100/0/0	425.8	75.9/9.25/14.8

References

[1] M. Krack, L. Salles, F. Thouverez, Vibration prediction of bladed disks coupled by friction joints, Arch. Comput. Methods Eng. 24 (2017) 589–636, http://dx.doi.org/10.1007/s11831-016-9183-2.

[2] A.V. Srinivasan, Flutter and resonant vibration characteristics of engine blades, J. Eng. Gas Turbines Power 119 (1997) 742, http://dx.doi.org/10.1115/1.2817053, URL http://gasturbinespower.asmedigitalcollection.asme.org/article.aspx?articleid=1420393.

[3] S. Schwarz, L. Kohlmann, A. Hartung, J. Gross, M. Scheel, M. Krack, Validation of a turbine blade component test with frictional contacts by phase-locked-loop and force-controlled measurements, J. Eng. Gas Turbines Power (2019) http://dx.doi.org/10.1115/1.4044772.

[4] D. Botto, F. Cuccovillo, V. Iannotti, Experimental investigation of friction damping in blade root joints, J. Eng. Gas Turbines Power (2022) 1–26, http://dx.doi.org/10.1115/1.4056099.

[5] J. Yuan, L. Salles, D. Nowell, C. Schwingshackl, Influence of mesoscale friction interface geometry on the nonlinear dynamic response of large assembled structures, Mech. Syst. Signal Process. 187 (2023) 109952, http://dx.doi.org/10.1016/j.ymssp.2022.109952, URL https://linkinghub.elsevier.com/retrieve/pii/S0888327022010202.

[6] R. Ahmed, C.M. Firrone, S. Zucca, A test rig for the full characterization of the dynamics of shrouded turbine blades, Mech. Syst. Signal Process. 189 (2023) 110080, http://dx.doi.org/10.1016/j.ymssp.2022.110080, URL https://linkinghub.elsevier.com/retrieve/pii/S0888327022011487.

[7] X. Guo, K. Ni, H. Ma, J. Zeng, Z. Wang, B. Wen, Dynamic response analysis of shrouded blades under impact-friction considering the influence of passive blade vibration, J. Sound Vib. 503 (2021) http://dx.doi.org/10.1016/j.jsv.2021.116112.

[8] D. Ye, F. Duan, J. Jiang, Z. Cheng, G. Niu, P. Shan, J. Zhang, Synchronous vibration measurements for shrouded blades based on fiber optical sensors with lenses in a steam turbine, Sensors 19 (2019) 2501, http://dx.doi.org/10.3390/s19112501, URL https://www.mdpi.com/1424-8220/19/11/2501.

[9] W. Gu, Z. Xu, Y. Liu, A method to predict the non-linear vibratory response of bladed disc system with shrouded dampers, Proc. Inst. Mech. Eng. Part C: J. Mech. Eng. Sci. 226 (2012) 1620–1632, http://dx.doi.org/10.1177/0954406211424671.

[10] C. Gastaldi, J. Gross, M. Scheel, T.M. Berruti, M. Krack, Modeling complex contact conditions and their effect on blade dynamics, J. Eng. Gas Turbines Power 143 (2021) http://dx.doi.org/10.1115/1.4049186.

[11] M. Umer, D. Botto, Measurement of contact parameters on under-platform dampers coupled with blade dynamics, Int. J. Mech. Sci. 159 (2019) 450–458, http://dx.doi.org/10.1016/j.ijmecsci.2019.06.010.

[12] L. Pesaresi, L. Salles, A. Jones, J.S. Green, C.W. Schwingshackl, Modelling the nonlinear behaviour of an underplatform damper test rig for turbine applications, Mech. Syst. Signal Process. 85 (2017) 662–679, http://dx.doi.org/10.1016/j.ymssp.2016.09.007.

[13] C.W. Schwingshackl, E.P. Petrov, D.J. Ewins, Effects of contact interface parameters on vibration of turbine bladed disks with underplatform dampers, J. Eng. Gas Turbines Power 134 (2012) 032507, http://dx.doi.org/10.1115/1.4004721, URL http://gasturbinespower.asmedigitalcollection.asme.org/article.aspx?articleid=1429804.

[14] R. Umehara, S. Takei, T. Akaki, H. Kitada, New modeling combining kinematic and stiffness nonlinearity in under platform dampers, in: Proceedings of ASME Turbo Expo 2021 Turbomachinery Technical Conference and Exposition, 2021.

[15] A. Mathis, N.N. Balaji, R. Kuether, A. Brink, M.R. Brake, D.D. Quinn, A review of damping models for structures with mechanical joints, Appl. Mech. Rev. (2020) http://dx.doi.org/10.1115/1.4047707.

[16] N.N. Balaji, M.R. Brake, The surrogate system hypothesis for joint mechanics, Mech. Syst. Signal Process. Accepted (2019) 42–64, http://dx.doi.org/10.1016/j.ymssp.2019.02.013.

[17] R. Lacayo, L. Pesaresi, J. Gross, D. Fochler, J. Armand, L. Salles, C.W. Schwingshackl, M.S. Allen, M.R. Brake, Nonlinear modeling of structures with bolted joints : a comparison of two approaches based on a time-domain and frequency-domain solver, Mech. Syst. Signal Process. (2019) 413–438.

[18] M. Krack, M.R. Brake, C. Schwingshackl, J. Gross, P. Hippold, M. Lasen, D. Dini, L. Salles, M.S. Allen, D. Shetty, C.A. Payne, K. Willner, M. Lengger, M.Y. Khan, J. Ortiz, D.A. Najera-Flores, R.J. Kuether, P.R. Miles, C. Xu, H. Yang, H. Jalali, J. Taghipour, H.H. Khodaparast, M.I. Friswell, P. Tiso, A.A. Morsy, A. Bhattu, S. Hermann, N. Jamia, H.N. Özgüven, F. Müller, M. Scheel, The tribomechadynamics research challenge: Confronting blind predictions for the linear and nonlinear dynamics of a thin-walled jointed structure with measurement results, Mech. Syst. Signal Process. 224 (2025) 112016, http://dx.doi.org/10.1016/j.ymssp.2024.112016, URL https://linkinghub.elsevier.com/retrieve/pii/S0888327024009142.

[19] R. de O. Teloli, P. Butaud, G. Chevallier, S. da Silva, Good practices for designing and experimental testing of dynamically excited jointed structures: The orion beam, Mech. Syst. Signal Process. 163 (2022) 108172, http://dx.doi.org/10.1016/j.ymssp.2021.108172, URL https://linkinghub.elsevier.com/retrieve/pii/S0888327021005495.

[20] C. Gastaldi, T.M. Berruti, M.M. Gola, A. Bessone, Experimental investigation on real under-platform dampers: the impact of design and manufacturing, in: Proceedings of ASME Turbo Expo 2019, 2019.

[21] M.R. Brake, C.W. Schwingshackl, P. Reuß, Observations of variability and repeatability in jointed structures, Mech. Syst. Signal Process. 129 (2019) 282–307, http://dx.doi.org/10.1016/j.ymssp.2019.04.020.

[22] C. Gastaldi, T. Berruti, M.M. Gola, The effect of surface finish on the proper functioning of underplatform dampers, J. Vib. Acoust. (2020) 1–30, http://dx.doi.org/10.1115/1.4046954.

[23] A. Fantetti, D. Botto, S. Zucca, C. Schwingshackl, Guidelines to use input contact parameters for nonlinear dynamic analysis of jointed structures: Results of a round robin test, Tribol. Int. 191 (2024) http://dx.doi.org/10.1016/j.triboint.2023.109158.

[24] C. Gastaldi, T.M. Berruti, M.M. Gola, A novel test rig for friction parameters measurement on underplatform dampers, Int. J. Solids Struct. 185–186 (2020) 170–181, http://dx.doi.org/10.1016/j.ijsolstr.2019.08.030, URL http://www.sciencedirect.com/science/article/pii/S0020768319303981.

[25] T. Wei, A. Fantetti, F. Cegla, C. Schwingshackl, An optical method to monitor transparent contact interfaces during high frequency shear vibration cycles, Wear (2023) 204840, http://dx.doi.org/10.1016/j.wear.2023.204840, URL https://linkinghub.elsevier.com/retrieve/pii/S0043164823002235.

[26] A. Fantetti, S. Mariani, L. Pesaresi, D. Nowell, F. Cegla, C. Schwingshackl, Ultrasonic monitoring of friction contacts during shear vibration cycles, Mech. Syst. Signal Process. 161 (2021) 107966, http://dx.doi.org/10.1016/j.ymssp.2021.107966, URL https://linkinghub.elsevier.com/retrieve/pii/S0888327021003617.

[27] H. Zhang, J. Tang, J. Liu, C. Li, T. Jia, Q. Gu, Modeling method and dynamic analysis of blade with double friction damping structure considering time-varying pressure distribution, J. Sound Vib. (2024) 118614, http://dx.doi.org/10.1016/j.jsv.2024.118614, URL https://linkinghub.elsevier.com/retrieve/pii/S0022460X24003766.

[28] A. Fantetti, R. Setchfield, C. Schwingshackl, Nonlinear dynamics of turbine bladed disk with friction dampers: Experiment and simulation, Int. J. Mech. Sci. 257 (2023) http://dx.doi.org/10.1016/j.ijmecsci.2023.108510.

[29] M. Wall, M.S. Allen, R.J. Kuether, Observations of modal coupling due to bolted joints in an experimental benchmark structure, Mech. Syst. Signal Process. 162 (2022) 107968, http://dx.doi.org/10.1016/j.ymssp.2021.107968.

[30] T. Dreher, M.R. Brake, B. Seeger, M. Krack, In situ, real-time measurements of contact pressure internal to jointed interfaces during dynamic excitation of an assembled structure, Mech. Syst. Signal Process. 160 (2021) http://dx.doi.org/10.1016/j.ymssp.2021.107859.

[31] P. Ranjan, A.K. Pandey, Effect of misaligned plates and varying interfacial area on bolted structures, Int. J. Mech. Sci. 233 (2022) http://dx.doi.org/10.1016/j.ijmecsci.2022.107640.

[32] V. Gimpl, A. Fantetti, S.W. Klaassen, C.W. Schwingshackl, D.J. Rixen, Contact stiffness of jointed interfaces: A comparison of dynamic substructuring techniques with frictional hysteresis measurements, Mech. Syst. Signal Process. 171 (2022) 108896, http://dx.doi.org/10.1016/j.ymssp.2022.108896, URL https://linkinghub.elsevier.com/retrieve/pii/S088832702200084X.

[33] H. Liu, W. Sun, D. Du, X. Liu, H. Ma, Nonlinear vibration of mistuning bolted composite plates considering stick-slip-separation characteristics, Int. J. Mech. Sci. (2023) 108126, http://dx.doi.org/10.1016/j.ijmecsci.2023.108126, URL https://linkinghub.elsevier.com/retrieve/pii/S0020740323000280.

[34] G. Zara, E. Ferhatoglu, T.M. Berruti, S. Zucca, Robust design of turbine blades with friction contacts in the presence of multiple response levels, Int. J. Non-Linear Mech. 164 (2024) 104770, http://dx.doi.org/10.1016/j.ijnonlinmec.2024.104770, URL https://linkinghub.elsevier.com/retrieve/pii/S0020746224001355.

[35] E. Ferhatoglu, C. Gastaldi, D. Botto, S. Zucca, An experimental and computational comparison of the dynamic response variability in a turbine blade with under-platform dampers, Mech. Syst. Signal Process. 172 (2022) http://dx.doi.org/10.1016/j.ymssp.2022.108987.

[36] C. Li, H. She, Q. Tang, B. Wen, The coupling vibration characteristics of a flexible shaft-disk-blades system with mistuned features, Appl. Math. Model. 67 (2019) 557–572, http://dx.doi.org/10.1016/j.apm.2018.09.041.

[37] H. She, C. Li, Q. Tang, B. Wen, The investigation of the coupled vibration in a flexible-disk blades system considering the influence of shaft bending vibration, Mech. Syst. Signal Process. 111 (2018) 545–569, http://dx.doi.org/10.1016/j.ymssp.2018.03.044.

[38] L.R. Tamatam, D. Botto, S. Zucca, A coupled approach to model wear effect on shrouded bladed disk dynamics, Int. J. Mech. Sci. (2023) 107816, http://dx.doi.org/10.1016/j.ijmecsci.2022.107816.

[39] L. Panning, K. Popp, W. Sextro, F.G. Otting, A. Kayser, I. Wolter, Asymmetrical underplatform dampers in gas turbine bladings: theory and application, in: Proceedings of ASME Turbo Expo, 2004.

[40] M. Wen, C. Zhang, J. Jing, T. Liu, Q. Lv, J. Li, Modal characteristics of blade-disk including rough interfaces and geometric deviations, Int. J. Mech. Sci. (2024) 109269, http://dx.doi.org/10.1016/j.ijmecsci.2024.109269, URL https://linkinghub.elsevier.com/retrieve/pii/S0020740324003114.

[41] E. Ferhatoglu, D. Botto, S. Zucca, Parametric study for model calibration of a friction-damped turbine blade with multiple test data, Nonlinear Dynam. (2024) http://dx.doi.org/10.1007/s11071-024-09396-z, URL https://link.springer.com/10.1007/s11071-024-09396-z.

[42] M.M. Gola, On comparing behavior and performance of underplatform dampers according to shape, J. Struct. Dyn. (2024) http://dx.doi.org/10.25518/2684-6500.239, URL https://popups.uliege.be/2684-6500/index.php?id=239.

[43] J. Armand, L. Pesaresi, L. Salles, C.W. Schwingshackl, A multi-scale approach for nonlinear dynamic response predictions with fretting wear, J. Eng. Gas Turbines Power 139 (2017) 1–7, http://dx.doi.org/10.1115/GT2016-56201, URL http://proceedings.asmedigitalcollection.asme.org/proceeding.aspx?doi=10.1115/GT2016-56201.

[44] L. Pesaresi, A. Fantetti, F. Cegla, L. Salles, C. Schwingshackl, On the use of ultrasound waves to monitor the local dynamics of friction joints, Exp. Mech. 60 (2020) 129–141, http://dx.doi.org/10.1007/s11340-019-00550-y, URL http://link.springer.com/10.1007/s11340-019-00550-y.

[45] A.A. Morsy, P. Tiso, Predicting the variability of the dynamics of bolted joints using polynomial chaos expansion, Mech. Syst. Signal Process. 224 (2025) 112008, http://dx.doi.org/10.1016/j.ymssp.2024.112008, URL https://linkinghub.elsevier.com/retrieve/pii/S0888327024009063.

[46] T. Butlin, G. Spelman, P. Ghaderi, W.J. Midgley, R. Umehara, Predicting response bounds for friction-damped gas turbine blades with uncertain friction coupling, J. Sound Vib. 440 (2019) 399–411, http://dx.doi.org/10.1016/j.jsv.2018.08.037, URL https://linkinghub.elsevier.com/retrieve/pii/S0022460X18305418.

[47] J. Yuan, A. Fantetti, E. Denimal, S. Bhatnagar, L. Pesaresi, C. Schwingshackl, L. Salles, Propagation of friction parameter uncertainties in the nonlinear dynamic response of turbine blades with underplatform dampers, Mech. Syst. Signal Process. 156 (2021) http://dx.doi.org/10.1016/j.ymssp.2021.107673.

[48] Y. Wu, H. Xuan, C. Wu, D. Mi, Effect of under-platform dampers on the forced vibration of high-speed rotating blades, J. Mech. Sci. Technol. 36 (2022) 3837–3850, http://dx.doi.org/10.1007/s12206-022-0707-4.

[49] V.N. Yakovkin, V.A. Besschetnov, Verification of a mathematical model of a dry friction damper for a GTE blade, in: Journal of Physics: Conference Series, vol. 1891, IOP Publishing Ltd, 2021, http://dx.doi.org/10.1088/1742-6596/1891/1/012037.

[50] D. Zhang, B. Gao, J. Hong, J. Fu, X. Ge, Experimental investigation on dynamic response of flat blades with underplatform dampers, Chin. J. Aeronaut. 32 (2019) 2667–2678, http://dx.doi.org/10.1016/j.cja.2019.04.022, URL http://www.sciencedirect.com/science/article/pii/S1000936119302122.
[51] D. Li, D. Botto, C. Xu, T. Liu, M.M. Gola, A micro-slip friction modeling approach and its application in underplatform damper kinematics, Int. J. Mech. Sci. 161–162 (2019) 105029, http://dx.doi.org/10.1016/j.ijmecsci.2019.105029, URL https://linkinghub.elsevier.com/retrieve/pii/S0020740319313979.
[52] M. Nikhamkin, N. Sazhenkov, S. Semenov, I. Semenova, An experimental technique to investigate gas-turbine blades dry-friction dampers efficiency, Adv. Mater. Struct. Eng. (2016) 71–75, http://dx.doi.org/10.1201/b20958-17.
[53] E. Cigeroglu, N.A.C.H. An, C.H. Menq, Forced response prediction of constrained and unconstrained structures coupled through frictional contacts, J. Eng. Gas Turbines Power 131 (2009) http://dx.doi.org/10.1115/1.2940356.
[54] J. Szwedowicz, C. Gibert, T.P. Sommer, R. Kellerer, Numerical and experimental damping assessment of a thin-walled friction damper in the rotating setup with high pressure turbine blades, J. Eng. Gas Turbines Power 130 (2008) 012502, http://dx.doi.org/10.1115/1.2771240.
[55] A. Fantetti, C. Gastaldi, T. Berruti, Modelling and testing flexible friction dampers : challenges and peculiarities, Exp. Tech. 42 (2018) 407–419, http://dx.doi.org/10.1007/s40799-018-0248-z.
[56] T. Hoffmann, L. Panning, J. Wallaschek, Measured and simulated forced response of a rotating turbine disk with asymmetric and cylindrical underplatform dampers, J. Eng. Gas Turbines Power (2020) http://dx.doi.org/10.1115/1.4045337.
[57] F. Nyssen, Y. Colaïtis, A. Batailly, Numerical investigation of a mistuned industrial bladed disk dynamics with structural contacts using time and frequency methods, J. Sound Vib. (2022) 117077, http://dx.doi.org/10.1016/j.jsv.2022.117077.
[58] F. Götting, W. Sextro, L. Panning, K. Popp, Systematic mistuning of bladed disk assemblies with friction contacts, in: Proceedings of the ASME Turbo Expo 2004, 2004.
[59] E.P. Petrov, A high-accuracy model reduction for analysis of nonlinear vibrations in structures with contact interfaces, J. Eng. Gas Turbines Power 133 (2011) 102503, http://dx.doi.org/10.1115/1.4002810, URL http://gasturbinespower.asmedigitalcollection.asme.org/article.aspx?articleid=1429551.
[60] M. Krack, G. Johann, Harmonic Balance for Nonlinear Vibration Problems, Springer Cham, 2019, http://dx.doi.org/10.1007/978-3-030-14023-6.
[61] G. Liu, Z. Lei, S.S. Law, Q. Yang, The nonlinear behavior of prestressed tuned mass damper for vibration control of wind turbine towers, Nonlinear Dynam. 111 (2023) 10939–10955, http://dx.doi.org/10.1007/s11071-023-08434-6.
[62] E.P. Petrov, D.J. Ewins, Analytical formulation of friction interface elements for analysis of nonlinear multi-harmonic vibrations of bladed disks, J. Turbomach. 125 (2003) 364, http://dx.doi.org/10.1115/1.1539868, URL http://turbomachinery.asmedigitalcollection.asme.org/article.aspx?articleid=1466592.
[63] Y. Yuan, A. Jones, R. Setchfield, C. Schwingshackl, Robust design optimisation of underplatform dampers for turbine applications using a surrogate model, J. Sound Vib. (2020) 115528, http://dx.doi.org/10.1016/j.jsv.2020.115528.
[64] C. Gastaldi, A. Fantetti, T. Berruti, Forced response prediction of turbine blades with flexible dampers: The impact of engineering modelling choices, Appl. Sci. 8 (2018) http://dx.doi.org/10.3390/app8010034, URL http://www.mdpi.com/2076-3417/8/1/34.
[65] A. Fantetti, L. Tamatam, M. Volvert, I. Lawal, L. Liu, L. Salles, M.R. Brake, C. Schwingshackl, D. Nowell, The impact of fretting wear on structural dynamics: Experiment and simulation, Tribol. Int. 138 (2019) 111–124, http://dx.doi.org/10.1016/j.triboint.2019.05.023.
[66] A. Fantetti, C. Schwingshackl, Effect of friction on the structural dynamics of built-up structures: An experimental study, in: Proceedings of the ASME Turbo Expo 2020: Turbomachinery Technical Conference and Exposition. Volume 11: Structures and Dynamics: Structural Mechanics, Vibration, and Damping; Supercritical CO2, 2020, http://dx.doi.org/10.1115/GT2020-14945.
[67] A. Fantetti, D. Botto, C. Schwingshackl, S. Zucca, Experimental dataset from a round robin test of contact parameters and hysteresis loops for nonlinear dynamic analysis, Data Brief (2024) http://dx.doi.org/10.1016/j.triboint.2023.109158.
[68] S. Medina, D. Nowell, D. Dini, Analytical and numerical models for tangential stiffness of rough elastic contacts, Tribol. Lett. 49 (2013) 103–115, http://dx.doi.org/10.1007/s11249-012-0049-y.
[69] ISO 2768 [internet], 2021, Available from: https://www.plianced.com/compliance-wiki/iso-2768-general-geometrical-tolerances-and-technical-drawings/. (Accessed 26 May 2021).